AIP | Applied Physics Letters

Moisture assisted perovskite film growth for high performance solar cells

Jingbi You, Yang (Michael) Yang, Ziruo Hong, Tze-Bin Song, Lei Meng, Yongsheng Liu, Chengyang Jiang, Huanping Zhou, Wei-Hsuan Chang, Gang Li, and Yang Yang

Citation: Applied Physics Letters **105**, 183902 (2014); doi: 10.1063/1.4901510
View online: http://dx.doi.org/10.1063/1.4901510
View Table of Contents: http://scitation.aip.org/content/aip/journal/apl/105/18?ver=pdfcov
Published by the AIP Publishing

Moisture assisted perovskite film growth for high performance solar cells

Jingbi You,[1] Yang (Michael) Yang,[1] Ziruo Hong,[1] Tze-Bin Song,[1] Lei Meng,[1] Yongsheng Liu,[1] Chengyang Jiang,[1] Huanping Zhou,[1] Wei-Hsuan Chang,[1] Gang Li,[1] and Yang Yang[1,2,a)]
[1]*Department of Materials Science and Engineering, University of California Los Angeles, Los Angeles, California 90095, USA*
[2]*California NanoSystems Institute, University of California Los Angeles, Los Angeles, California 90095, USA*

(Received 13 October 2014; accepted 30 October 2014; published online 7 November 2014)

Moisture is assumed to be detrimental to organometal trihalide perovskite, as excess water can damage the crystallinity of the perovskite structure. Here, we report a growth mode for via thermal annealing of the perovskite precursor film in a humid environment (e.g., ambient air) to greatly improve the film quality, grain size, carrier mobility, and lifetime. Our method produces devices with maximum power conversion efficiency of 17.1% and a fill factor of 80%, revealing a promising route to achieve high quality perovskite polycrystalline films with superior optoelectronic properties that can pave the way towards efficient photovoltaic conversion. © *2014 AIP Publishing LLC*.
[http://dx.doi.org/10.1063/1.4901510]

Perovskite type semiconductors, due to their excellent absorption and charge transport, have attracted a significant amount of attention in recent years.[1,2] Miyasaka *et al*. demonstrated the first lead halide perovskite photovoltaic device as the light absorber in a dye-sensitized solar cell, yielding a power conversion efficiency (PCE) of 4%.[2] However, it was later realized that the liquid electrolyte hole transport material resulted in degradation of the perovskite layer.[2,3] Further progress was made within a few years by employing mesoporous nanostructure that boosted the PCE well above 10%.[4–9] These results suggest an enormous potential for perovskite compounds as efficient photoactive materials for photovoltaic applications.[10–17]

Lead halide perovskite films can be deposited onto the substrates through *in situ* reactions of precursors via single- or two-step methods.[2–28] Initially, mesoporous metal oxides, either semi-conductive or insulating, were used to form continuous high-quality perovskite films in photovoltaic devices.[3–9] To simplify the device architecture and processing procedures, planar architectures without mesoporous layers have been proposed.[18–20] In the meantime, photo-physical studies have shown that perovskite materials exhibit several tens of nanoseconds in carrier lifetimes and a few hundred nanometers in diffusion lengths, justifying the use of planar hetero-junctions.[21,22] Intriguingly, perovskite materials demonstrate bipolar transport properties[20] and can be readily incorporated into p-i-n device architectures where they serve as the intrinsic absorption layer. Recent works demonstrated that solution and vacuum co-evaporation processing techniques delivered PCEs of 12%[19,23–27] and 12%–15%[20,28] in planar designs, respectively. Although the growth dynamics of perovskite films are far less understood at present, the simplicity of one-step solution processing techniques makes them preferable to two-step methods. It is critical to gain a deep insight into film growth mechanisms to enable use of facile one-step processing methods that can produce high-quality perovskite films. Previous reports show that full coverage of the perovskite film on the substrate surface is necessary to ensure sufficient shunt resistance. Coverage can be improved by annealing the film to fuse separate crystals into one and also by increasing film thickness.[19] Similar processes are essential to reduce structural defects and electronic traps within thin film solar cells. Unfortunately, perovskites cannot withstand temperatures above 110 °C, at which they are susceptible to decomposition or de-wetting.[19] Film thickness is also limited by the charge diffusion length as indicated by the deterioration of photovoltaic performance for thicker layers. In order to address these challenges, we must develop effective approaches for controlling the crystal growth using facile and controllable deposition conditions.[29–31]

In this letter, we report moisture assisted grain growth of solution processed perovskite films. As an approach to achieve high-quality perovskite films, we anneal the precursor film in a humid environment (ambient air) to dramatically increase grain size, carrier mobility, and charge carrier lifetime, thus improving electrical and optical properties and enhancing photovoltaic performance. We demonstrate perovskite solar cells with 17.1% PCE and a fill factor (FF) of 80%.

The details of device fabrication can be found in our previous publication.[24] Specifically, the mixture solution of 1:3 ratio of $PbCl_2$:CH_3NH_3I in *N*,*N*-dimethylformamide (DMF) solvent (0.8M) was spin coated onto the poly(3,4-ethylenedioxythiophene) polystyrene sulfonate (PEDOT:PSS) layer at 1500 rpm. The precursor film are annealing at 90 °C for 2 h in nitrogen glove box or dry oxygen glove box or ambient air (humidity of 35% ± 5%). To study the effect of moisture level on the morphology and devices' performance, the samples are placed into the humid controllable chamber for annealing. After annealing, the perovskite films were transferred into nitrogen glove box. A 2% phenyl-C61-butyric acid methyl ester (PCBM) in chlorobenzene solution was coated onto the perovskite layer at 1000 rpm. After that, 0.02% polyelectrolyte poly[(9,9-bis(3′-(*N*,*N*-dimethylamino) propyl)-2,7-fluorene)-alt-2,7-(9,9-dioctylfluorene)] (PFN) in

a)Author to whom correspondence should be addressed. Electronic mail: yangy@ucla.edu

methanol was spin-coated on PCBM at 2000 rpm. Finally, the device was transferred to vacuum chamber for Al electrode evaporation. The devices' area is 0.1 cm^2. The X-ray diffraction (XRD) patterns were collected on a PANalytical X'Pert Pro X-ray powder diffractometer using Cu-Kα radiation ($\lambda = 1.54050$ Å). The scanning electron microscope (SEM) images were taken on a Jeooel JSM-6700F. Steady-state photoluminescence (PL) was measured by Horiba Jobinyvon system with an excitation at 600 nm. External quantum efficiencies (EQE) were measured by an Enli Technology (Taiwan) EQE measurement system.

The SEM images of the perovskite films fabricated via the thermal annealing method (90 °C, 2 h in nitrogen glove box, O_2 and H_2O level lower than 5 ppm) are shown in Figs. 1(a) and 1(b). The pristine film exhibits a grain size of 100–300 nm with apparent pin holes and grain boundaries. These defects introduce strong energetic disorder, which impedes the charge transport, induces recombination, and lowers photovoltaic performance.[19] Significant improvement in film morphology results when perovskite precursor films are annealed in ambient air (humidity of 35% ± 5%). Perovskite films annealed in ambient air are shown in Figs. 1(c) and 1(d), respectively. Notably, individual crystal sizes have been increased, pin-holes have been significantly reduced, and grain sizes increased beyond 500 nm. On the other hand, when annealing the perovskite precursor film in a dry oxygen environment (Figs. 1(e) and 1(f)), the film morphology is similar as in the case of the nitrogen environment, indicating the significant role of moisture on the final film morphology. The cross-section SEM showed that the crystal change across the entire of perovskite film (Fig. S1, in Ref. 32). XRD results confirm the improved crystallinity of the perovskite films (Fig. S2, in Ref. 32), as the diffraction peaks of films annealed in a humid environment are stronger and sharper than those annealed in a dry nitrogen environment.

To further confirm our hypothesis, the perovskite precursor films were annealed in a humid nitrogen chamber. Similarly, large crystals and fewer pin-holes are seen than that of the dry nitrogen environment (Fig. S3, in Ref. 32). This result directly confirmed that the moisture introduction is helpful for perovskite film growth. Furthermore, we systematically studied the effect of moisture level (20%–80% humidity) on the perovskite film formation (Fig. S4, in Ref. 32). Despite the contributions of humidity in constructing larger crystal sizes, XRD results show a small amount of PbI_2 phase present in crystals after annealing above 80% humidity. This may be an indication that the $CH_3NH_3PbI_3$ decomposes under high humidity levels (Fig. S5, in Ref. 32). We can conclude that while moisture is beneficial for high quality perovskite film growth, the relative amount should be carefully controlled.

Moisture-assisted crystal growth has previously been seen in various crystal systems, inducing grain boundary creep as a result of the absorption of moisture within the grain boundaries.[33–35] Due to the strong hydroscopic nature of CH_3NH_3I,[36] exposing perovskite precursor to moisture during film formation could results in accumulation of moisture within grain boundaries, inducing grain boundary creep and subsequently merging adjacent grains together. This effectively increases grain size and reduces pinhole formation. In addition to grain boundary movement, moisture could also provide an aqueous environment to enhance the diffusion length of the precursor ions, further promoting perovskite grain growth. The recrystallization process via moisture annealing give rise to a high quality perovskite film, a proposed scheme for enhanced crystallinity of perovskite film in moisture environment is shown in Fig. S6 (in Ref. 32). The accurate of moisture-assisted perovskite growth is not clear and still under study.

Figure 2(a) shows steady-state PL measurement for precursor films annealed under varying atmospheric conditions, such as nitrogen, oxygen, and ambient air (humidity: 35% ± 5%), the PL results are shown in Fig. 2(a). The perovskite film was deposited via spin-coating onto a layer of PEDOT:PSS to emulate real p-i-n device processing conditions. The enhanced PL indicates that the non-radiative decay is significantly suppressed through our annealing method. Furthermore, time-resolved PL (TRPL) (Fig. 2(b)) clearly shows that PL lifetime improves with annealing in ambient air. Annealing in a dry nitrogen and oxygen environment gave lifetimes of approximately 33 ns, whereas the humidity-controlled annealing increased the lifetime to ~91 ns. Here, the PL and the TRPL measurements show that the non-radiative recombination channels are greatly inhibited, and therefore the number of defects reduced, by annealing the precursor film in a humid environment.

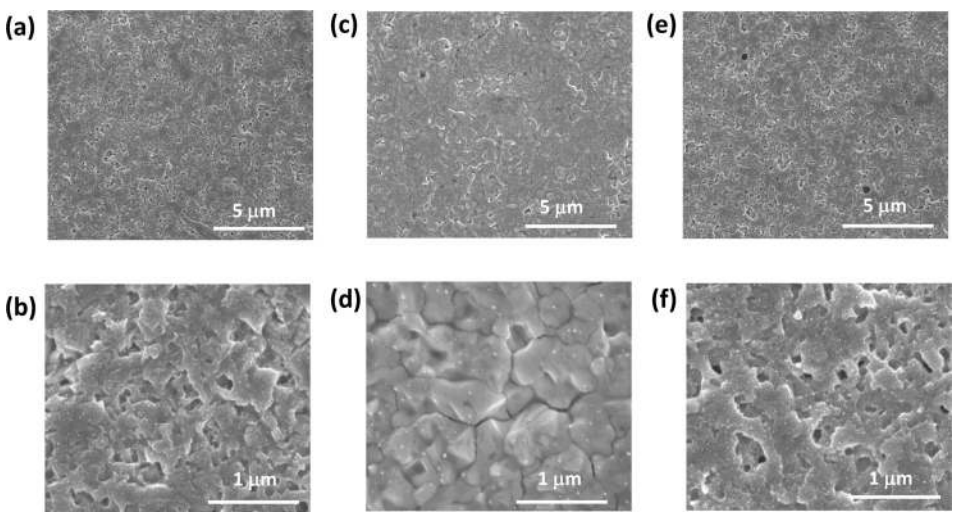

FIG. 1. SEM images of the perovskite film precursor films annealed under different conditions (a) and (b) in nitrogen; (c) and (d) in ambient air; (e) and (f) in oxygen environment. The small white dots in the SEM images are evaporated gold particles on perovskite film surface for reducing charge effect during SEM measurements.

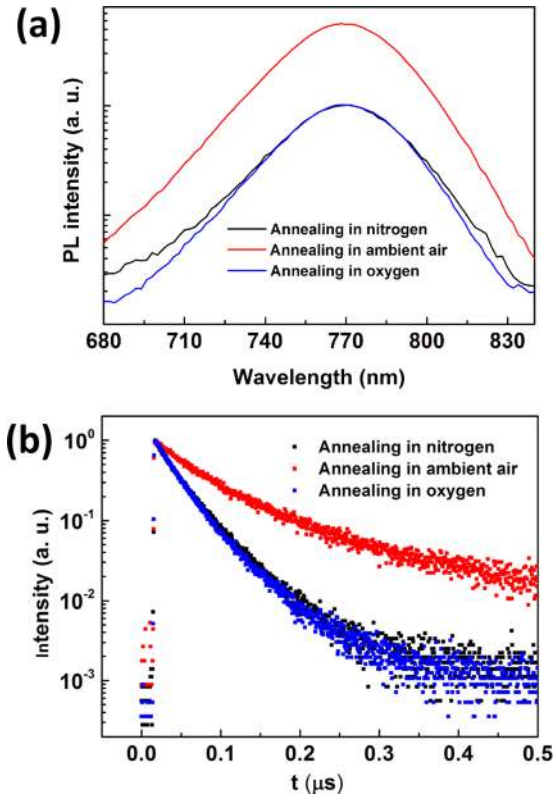

FIG. 2. The perovskite film with improved crystal quality confirmed by steady photoluminescence and transit photoluminescence. (a) Steady-state PL measurement of perovskite film annealed under different environment including nitrogen, ambient air, and oxygen, the films are all coated on PEDOT:PSS surface. (b) TRPL measurement for the corresponding perovskite films.

Using our annealing method, we constructed devices consisting of glass/ITO/PEDOT:PSS/$CH_3NH_3PbI_{3-x}Cl_x$/PCBM/PFN/Al as shown in Fig. 3(a), where PEDOT:PSS and PCBM are the hole and electron transport layers, respectively. We incorporated a layer of PFN to form an Ohmic contact to assist in electron extraction from the PCBM to Al.[37] This resulted in improved device performance, especially in FF (Fig. S7, in Ref. 32). The J-V characteristics of the devices based on perovskite films annealed in different environment are shown in Fig. 3(b). When the precursor film is annealed in dry environment, the device performance showed approximately 12% PCE. In comparison, we can see that when annealing precursor film in ambient air, the PCE is increased from 12.3% to 15.4%, the V_{OC} from 0.86 V to 0.99 V and FF from 75% to 78%, while the short circuit current (J_{SC}) maintained at 19 mA/cm^2. The best performance achieved through our annealing process was 17.1% PCE (Fig. 3(c)). The performance of the devices is summarized in Table I. External quantum efficiency (EQE) of the device is shown in Fig. 3(d). The integrated J_{SC} is 19.2 mA/cm^2, which is consistent with J-V measurement but for a small difference resulting from encapsulation degradation. Most notably, our method is robust and our results highly consistent and reproducible, which is unambiguously ascribed to the moisture effects during annealing (Fig. S8, in Ref. 32). Device performance of varying humidity levels are shown in Fig. S9 and Table S1 (in Ref. 32), depicting that moisture levels lower than 60% result in significant enhancements. Slight degradation occurs at humidity levels greater than 80%, particularly reducing the FF, which could be due to the presence of an inherent PbI_2 phase.

The improved V_{OC} and FF strongly indicate a reduction in recombination loss as a result of our annealing method. For further confirmation, the I-V characteristics of the devices treated under different conditions were analyzed. Planar structured perovskite solar cells can be treated as a single junction diode. For a device with a large shunt resistance (>3000 Ω·cm^2, the shunt resistance of the pristine and moisture treated devices both exceed 3000 Ω·cm^2),[38,39] the I-V characteristics are described by

$$J = J_{SC} - J_0\left[\exp\left(\frac{e(V + JR_s)}{AK_BT}\right) - 1\right], \qquad (1)$$

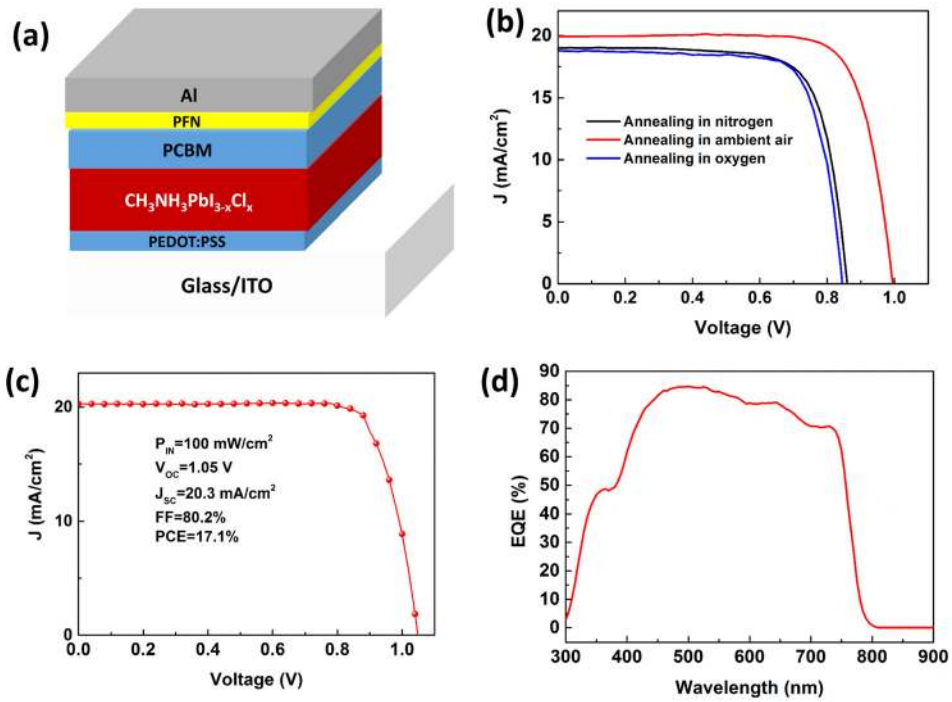

FIG. 3. Device structure and device performance. (a) The device structure glass/ITO/PEDOT:PSS/$CH_3NH_3PbI_{3-x}Cl_x$/PCBM/PFN/Al. (b) J-V curve of the corresponding devices with the perovskite films annealed under different environment, the measurements are carried out in simulated sunlight at 100 mW cm^{-2}. (c) J-V curve for a best-performance measured at 1 sun condition at 100 mW cm^{-2}. (d) External quantum efficiency of the corresponding devices.

TABLE I. Devices performance of perovskite films annealed under different environment. The device where the perovskite annealed in ambient air showed the best efficiency of 17.1%, the corresponding J-V is shown in Fig. 3(c), the parameters of the best device are also included in table. Our devices showed very good reproducibility, the histograms of devices PCE are shown in Figure S8.

Devices	V_{OC} (V)	J_{SC} (mA/cm^2)	FF (%)	PCE (%)
Annealing in nitrogen	0.86	19.0	75	12.3
Annealing in ambient air	0.99	19.9	78	15.4
Annealing in ambient air (best)	1.05	20.3	80.2	17.1
Annealing in oxygen	0.85	18.7	76	12.1

where J is the current flow through the external load, J_{SC} is the light induced current, J_0 is the dark saturate current density, V is the applied voltage, A is the ideality factor, K_B is the Boltzmann constant, T is the temperature, and e is the electron charge. Based on Eq. (1), the V_{OC} is obtained when the current flowing through the external circuit is zero

$$V_{OC} = \frac{AK_BT}{q} ln\left(\frac{J_{SC}}{J_0} + 1\right). \quad (2)$$

It can be seen through Eq. (2) that a higher V_{OC} corresponds to a lower J_0. Equation (1) can also be written as[38,39]

$$-\frac{dV}{dJ} = \frac{AK_BT}{e}(J_{SC} - J)^{-1} + R_s, \quad (3)$$

$$ln(J_{SC} - J) = \frac{e}{AK_BT}(V + R_SJ) + lnJ_0. \quad (4)$$

J_0 can be obtained by fitting the curve of $\ln(J_{SC}-J)$ vs $(V+R_SJ)$, where the Rs is obtained by fitting the curve of $-dV/dJ$ *vs* $(J_{SC}-J)^{-1}$. The J-V curves shown in Figure 3(b) were used for analysis. The plots of $-dV/dJ$ vs $(J_{SC}-J)^{-1}$ and $\ln(J_{SC}-J)$ *vs* $(V+R_SJ)$ are shown in Figures 4(a) and 4(b), respectively. Linear plot fitting of Figure 4(a) shows that the perovskite films annealed in nitrogen and ambient air exhibit similar series resistances ($\sim 1\,\Omega\cdot cm^2$). The series resistances of nitrogen and ambient air annealed samples show 0.9 and $1.4\,\Omega\cdot cm^2$, respectively; while the ideality factor calculated is close to 2.3 for the two devices. Similarly, by linearly fitting the $\ln(J_{SC}-J)$ *vs* $(V+R_SJ)$, the ideality factor are 2.3 for the films annealing in nitrogen and ambient air. The ideality factors obtained by the two methods are consistent. J_0 for the pristine and air ambient devices are 1.4×10^{-5} and 8.1×10^{-7} mA/cm^2, respectively. The J_0 from air annealed samples is $\sim$2 orders of magnitude lower than that of the pristine samples. J_0 is a well-understood parameter indicating the thermal emission rate of electrons from the valence band to the conduction band, and is directly related to the recombination rate. The smaller J_0 of the air exposed sample indicates a lower recombination loss, and accordingly a higher V_{OC} consistent with the measured high FF.

Finally, it must be noted that our devices showed no obvious I-V hysteresis, this is much different behavior from conventional planar structure devices based on TiO_2 transport layer,[40] the details can be found in supplementary material (Fig. S10, in Ref. 32).

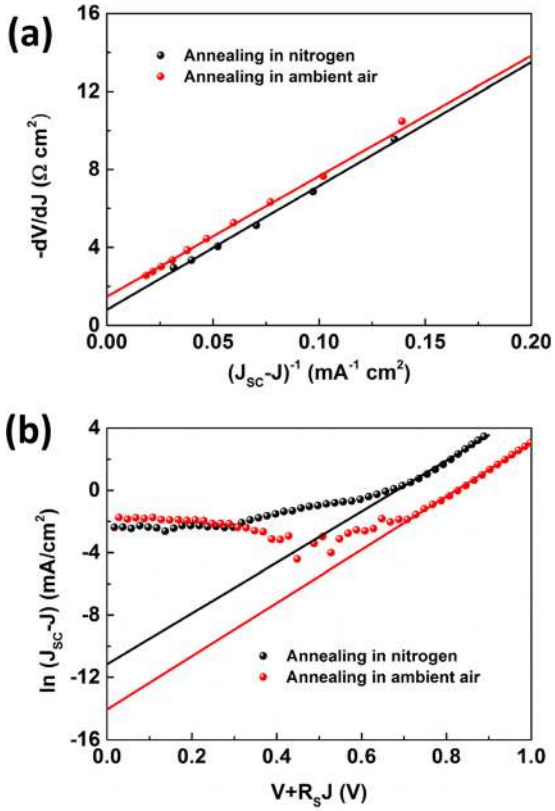

FIG. 4. I-V characteristic the devices where the precursor films are annealed in nitrogen and ambient air. (a) Plot of $-dV/dJ$ *vs* $(J_{SC}-J)^{-1}$ and linear fitting. (b) $\ln(J_{SC}-J)$ *vs* $(V+R_SJ)$ and linear fitting. Both of them fitting are located around corresponding V_{OC}. The original J-V curve and device performance parameters are shown in Figure 3(b).

In conclusion, we reveal that mild moisture has a positive effect on perovskite film formation, demonstrating perovskite solar cells with 17.1% power conversion efficiencies, fill factors over 80%, and the elimination of hysteresis effects. The moisture induced perovskite grain growth method is not limited to solar cell application but applicable to other electronic devices, such as light-emitting diodes (LEDs), lasers, transistors and sensors.

This work was financially supported by the National Science Foundation (NSF-ECCS 1202231, Program Manager: Dr. Paul Werbos), Air Force Office of Scientific Research (grant no. FA9550-12-1-0074, Program Manager: Dr. C. Lee), and UCLA internal funds. The authors would like to thank Professor Xingwang Zhang from the Institute of Semiconductors for fruitful discussion on film growth. The authors would also like to thank Mr. Ding-Wen Chung and Nicholas De Marco for proof reading, Dr. Shirong Lu for synthesizing CH_3NH_3I compound, and Dr. Min Cai for providing PFN solution.

[1]C. R. Kagan, D. B. Mitzi, and C. D. Dimitrakopoulos, Science **286**, 945 (1999).
[2]A. Kojima, K. Teshima, Y. Shirai, and T. Miyasaka, J. Am. Chem. Soc. **131**, 6050 (2009).
[3]J.-H. Im, C. R. Lee, J. W. Lee, S. W. Park, and N. G. Park, Nanoscale **3**, 4088 (2011).
[4]H. S. Kim, C. R. Lee, J. H. Im, K. B. Lee, T. Moehl, A. Marchioro, S. Moon, R. Humphry-Baker, J. H. Yum, J. E. Moser, M. Gratzel, and N. G. Park, Sci. Rep. **2**, 591 (2012).

[5]M. M. Lee, J. Teuscher, T. Miyasaka, T. N. Murakami, and H. J. Snaith, Science **338**, 643 (2012).
[6]J. Burschka, N. Pellet, S. J. Moon, R. Humphry-Baker, P. Gao, M. K. Nazeeruddin, and M. Gratzel, Nature **499**, 316 (2013).
[7]L. Etgar, P. Gao, Z. S. Xue, Q. Peng, A. K. Chandiran, B. Liu, M. Nazeeuddin, and M. Graztel, J. Am. Chem. Soc. **134**, 17396 (2012).
[8]J. H. Heo, S. H. Im, J. H. Noh, T. N. Mandal, C. S. Lim, J. A. Chang, Y. H. Lee, H. J. Kim, A. Sarkar, M. K. Nazeeruddin, M. Gratzel, and S. Seok, Nat. Photonics **7**, 486 (2013).
[9]J. H. Noh, S. H. Im, J. H. Heo, T. N. Mandal, and S. I. Seok, Nano Lett. **13**, 1764 (2013).
[10]M. D. McGehee, Nature **501**, 323 (2013).
[11]R. F. Service, Science **342**, 794 (2013).
[12]G. Hodes, Science **342**, 317 (2013).
[13]N.-G. Park, J. Phys. Chem. Lett. **4**, 2423 (2013).
[14]P. V. Kamat, J. Phys. Chem. Lett. **4**, 3733 (2013).
[15]J. Bisquert, J. Phys. Chem. Lett. **4**, 2597 (2013).
[16]H. J. Snaith, J. Phys. Chem. Lett. **4**, 3623 (2013).
[17]T. Leijtens, G. E. Eperon, S. Pathak, A. Abate, M. M. Lee, and H. J. Snaith, Nat. Commun. **4**, 2885 (2013).
[18]J. Y. Jeng, Y. F. Chiang, M. H. Lee, S. R. Peng, T. F. Guo, P. Chen, and T. C. Wen, Adv. Mater. **25**, 3727 (2013).
[19]G. E. Eperon, V. M. Burlakov, P. Docampo, A. Goriely, and H. J. Snaith, Adv. Funct. Mater. **24**, 151 (2014).
[20]M. Liu, M. B. Johnston, and Snaith, Nature **501**, 395 (2013).
[21]S. D. Stranks, G. E. Eperon, G. Grancini, C. Menelaou, M. J. P. Alcocer, T. Leijtens, L. M. Herz, A. Petrozza, and H. J. Snaith, Science **342**, 341 (2013).
[22]G. C. Xing, N. Mathews, S. Y. Sun, S. S. Lim, Y. M. Lam, M. Gratzel, S. Mhaisalkar, and T. C. Sum, Science **342**, 344 (2013).
[23]Q. Chen, H. Zhou, Z. Hong, S. Luo, H. S. Duan, H. S. Wang, Y. Liu, G. Li, and Y. Yang, J. Am. Chem. Soc. **136**, 622 (2014).
[24]J. You, Z. Hong, Y. Yang, Q. Chen, M. Cai, T. Z. Song, C. C. Chen, S. R. Lu, Y. Liu, H. Zhou, and Y. Yang, ACS Nano **8**, 1674 (2014).
[25]S. Y. Sun, T. Salim, N. Mathews, M. Duchamp, C. Boothroyd, G. Xing, T. C. Sum, and Y. M. Lam, Energy Environ. Sci. **7**, 399 (2014).
[26]D. Y. Liu and T. L. Kelly, Nat. Photonics **8**, 133 (2014).
[27]B. Conings, L. Baeten, C. D. Dobbelaere, J. D'Haen, J. Manca, and H. G. Boyen, Adv. Mater. **26**, 2041 (2014).
[28]O. Malinkiewicz, A. Yella, Y. H. Lee, G. M. Espallargas, M. Graetzel, M. K. Nazeeruddin, and H. J. Bolink, Nat. Photonics **8**, 128 (2014).
[29]M. Xiao, F. Huang, W. Huang, Y. Dkhissi, Y. Zhu, J. Etheridge, A. G. Weale, U. Bach, Y. Cheng, and L. Spiccia, Angew. Chem., Int. Ed. **53**, 9898 (2014).
[30]N. J. Jeon, J. H. Noh, Y. C. Kim, W. S. Yang, S. Ryu, and S. Seok, Nat. Mater. **13**, 897 (2014).
[31]Z. G. Xiao, Q. F. Dong, C. Bi, Y. Shao, Y. Yuan, and J. Huang, Adv. Mater. **26**, 6503 (2014).
[32]See supplementary material at http://dx.doi.org/10.1063/1.4901510 for details about morphology, crystal structure , moisture level effect and devices measurement study (Figure S1-S10).
[33]J. L. Urai, Tectonophysics **96**, 125 (1983).
[34]J. L. Urai, C. J. Spiers, H. J. Zwart, and G. S. Lister, Nature **324**, 554 (1986).
[35]P. J. Anderson and P. L. Morgan, Trans. Faraday Soc. **60**, 930 (1964).
[36]G. Alagona, C. Ghio, and P. Kollman, J. Am. Chem. Soc. **108**, 185 (1986).
[37]Z. C. He, C. Zhong, X. Huang, W. Y. Wong, H. B. Wu, L. W. Chen, S. J. Su, and Y. Cao, Adv. Mater. **23**, 4636 (2011).
[38]J. R. Sites and P. H. Mauk, Sol. Cells **27**, 411 (1989).
[39]J. J. Shi, J. Dong, S. Lv, Y. Xu, L. Zhu, J. Xiao, X. Xu, H. Wu, D. Li, Y. Luo, and Q. Meng, Appl. Phys. Lett. **104**, 063901 (2014).
[40]H. J. Snaith, A. Abate, J. M. Ball, G. E. Eperon, T. Leijtens, N. K. Noel, S. D. Stranks, J. Wang, K. Wojciechowski, and W. Zhang, J. Phys. Chem. Lett. **5**, 1511 (2014).